Article ID: 1007-4627(2013) 03-0299-09

Quasifission in Heavy Ion Fusing Reaction Systems

YU Lin[1, 2], GAN Zaiguo[1], HUANG Minghui[1], ZHANG Hongfei[3], LI Junqing[1, 3]

(*1. Institute of Modern Physics, Chinese Academy of Sciences, Lanzhou 730000, China;*
2. University of Chinese Academy of Sciences, Beijing 100049, China;
3. School of Nuclear Science and Technology, Lanzhou University, Lanzhou 730000, China)

Abstract: In heavy ion fusion reactions, the quasifission(QF) is competing with fusion, and which is often described by incorporating the Kramers formula(KRA-F) into the master equation(ME) within the Di-Nuclear System(DNS) model. However the KRA-F works well only if the QF barrier is high enough. Presently by taking the relative distance of nuclei as an independent dynamical variable, the evolution of the DNS towards fusion and QF are both treated as a diffusion process in a consistent way by solving MEs. The validity of the KRA-F is thus checked. Furthermore, the dynamical deformation and the nucleon transfer in heavy ion fusion reaction process are viewed simultaneously as a diffusion process, and are treated by solving a set of MEs with the variables of the quadrupole deformation of each nucleus and the mass asymmetry variable in the potential energy surface(PES) of the system. The distinct influence of the dynamical deformation on the QF mass yield distribution is discussed, and the experimental observations can be well reproduced by the calculation.

Key words: superheavy nucleus; quasifission; fusion; master equation; driving potential

CLC number: O571.6 **Document code:** A **DOI:** 10.11804/NuclPhysRev.30.03.299

1 Introduction

The heaviest nuclei currently are produced by fusion-evaporation reactions[1–9], but the reaction mechanism is still not yet very clear. It is important to study the reaction mechanism for localizing the island of stability of the superheavy nucleus(SHN) experimentally. The compound nucleus does not provide any information about the reaction mechanism, while the quasifission(QF), which happens in the intermediate reaction stage, is closely related with the shell structure, deformation of the interacting nuclei, carries the information.

In the Di-Nuclear System(DNS) conception it is assumed that in heavy ion reactions the projectile overcomes the coulomb barrier, and the DNS is formed. The two nuclei are in touching configuration and will transfer nucleons between the nuclei to form a compound nucleus, or evolve along the internuclear distance and decay into two fragments without forming the compound nucleus. The nucleon transfer is described by the master equation(ME), and the fragment decay is usually described by incorporating a Kramers formula(KRA-F) into the ME[10–13]. Since the KRA-F is an approximate solution under the quasi-stationary condition of Fokker-Planck equation, which demands certain amount of QF barrier as comparing with the nuclear temperature, and it is not always fulfilled during the fusion process, and the validity of the KRA-F is checked. Furthermore, our study by taking the dynamical deformations of nuclei into account revealed that the dynamical deformation results are very agreeable QF mass yield with the data.

Received date: 10 Dec. 2012; **Revised date:** 14 Jun. 2013

Foundation item: National Natural Science Foundation of China(11120101005, 11175074, 11105035, 10805061, 10825522, 10975064); Knowledge Innovation Project of Chinese Academy of Sciences(KJCX2-EW-N01); National Basic Research Program of China(973 Program)(2007CB815000)

Biography: YU Lin(1988–), female, Taizhou, Jiangsu, Master, working on the synthesis mechanism of Superheavy nucleus; E-mail: yulin@impcas.ac.cn.

Corresponding author: LI Junqing, E-mail: jqli@impcas.ac.cn

The paper is organized as follows: first we introduce the formalism of the DNS in Section 2, then the treatment of QF by KRA-F is described in Section 3. The validity of the KRA-F to treat the QF is checked by two variable ME in Section 4. The effect of the dynamical deformation on the QF mass yield distribution is described in Section 5. In Section 6 we present our summary.

2 The DNS conception

In the DNS concept the evaporation residue cross section to produce SHN can be written as a sum over all partial waves J[14]:

$$\sigma_{\rm ER}(E_{\rm c.m.}) = \sum_{J=0}^{J=J_{\rm f}} \sigma_{\rm C}(E_{\rm c.m.},J)P_{\rm CN}(E_{\rm c.m.},J)W_{\rm sur}(E_{\rm c.m.},J)\ , \qquad (1)$$

which consists of three factors: $\sigma_{\rm C}(E_{\rm c.m.},J)$ is the capture cross-section to describe the projectile overcomes the Coulomb barrier to form a DNS with the target. The fusion probability $P_{\rm CN}(E_{\rm c.m.},J)$ is evaluated by considering the fusion process as a diffusion of DNS in the mass asymmetry $\eta=\dfrac{A_1-A_2}{A}$, with A_1, A_2 the mass numbers of the DNS nuclei, and $A=A_1+A_2$. The nucleon transfer is coupled with the dissipation of the relative kinetic energy and the angular momentum, and the relaxation of colliding nuclear deformations. The survival probability $W_{\rm sur}(E_{\rm c.m.},J)$ estimates the competition between fission and neutron evaporation of the excited compound nucleus by the statistical model and decreases much with increasing J, which determines the maximal contributing $J_{\rm f}$.

3 The QF mass yield distribution described by the KRA-F

Let $P(A_1,E_1,t)$ be the distribution function to find A_1 nucleons with excitation energy E_1 in fragment 1 at time t, where E_1 is not considered as an independent variable but a parameter supplied by the initial relative motion. $P(A_1,E_1,t)$ obeys the following ME:

$$\frac{{\rm d}P(A_1,E_1,t)}{{\rm d}t} = \sum_{A_1'} W_{A_1,A_1'}\left[d_{A_1}P(A_1',E_1',t)-d_{A_1'}P(A_1,E_1,t)\right] - \Lambda^{\rm QF}_{A_1,E_1,t}(\Theta)P(A_1,E_1,t)\ , \qquad (2)$$

where $W_{A_1,A_1'}=W_{A_1',A_1}$ is the mean transition probability from a channel (A_1,E_1) to (A_1',E_1'), d_{A_1} denotes the microscopic dimension for the corresponding macroscopic variables. The coefficient $\Lambda^{\rm QF}_{A_1,E_1,t}(\Theta)$ is the rate of decay probability in R, and will be described later. The sum is taken over all possible mass numbers that fragment 1 may take(from 0 to $A=A_1+A_2$). The excitation energy E_1 is determined by the dissipation energy from the relative motion and the PES of the DNS, which is given by ε^* in the following text. The motion of nucleons in the interacting potential is governed by the single-particle Hamiltonian[15−16].

In the relaxation process of the relative motion, the DNS will be excited by the dissipation of the relative kinetic energy. The local excitation energy is determined by the excitation energy of the composite system and the PES of the DNS. The PES of the DNS, i.e. the driving potential of the nucleon transfer is given by

$$U(A_1,\,A_2,\,J) = B(A_1)+B(A_2)+V_{\rm CN}(A_1,\,A_2,\,J) - \left[B(A_{\rm CN})+V^{\rm CN}_{\rm rot}(J)\right]\ , \qquad (3)$$

where $A_{\rm CN}=A_1+A_2$ is the mass number of the compound nucleus, $B(A_i),(i=1,2)$ and $B(A_{\rm CN})$ are the negative binding energies of the fragment i and the compound nucleus, respectively, in which the shell and the pairing corrections are included. The $V^{\rm CN}_{\rm rot}$ is the rotation energy of the compound nucleus. The interaction potential $V_{\rm CN}(A_1,A_2,J)$ between fragments includes the nuclear, Coulomb and centrifugal parts, the details are given in Ref.[16]. The distance between the nuclei is taken to be the value which gives the minimum potential energy. The excited system opens a valence space $\Delta\varepsilon_K$ in each fragment $K(K=1,2)$, which has a symmetrical distribution around the Fermi surface. Only the particles in the states within this valence space are actively involved in excitation and transfer.

$$\Delta\varepsilon_K=\sqrt{\frac{4\varepsilon_K^*}{g_K}},\ \ \varepsilon_K^*=\varepsilon^*\frac{A_K}{A},\ \ g_K=\frac{A_K}{12}, \qquad (4)$$

where the ε^* is the local excitation energy of the DNS, which provides the excitation energy for the mean transition probability. There are $N_K=g_K\Delta\varepsilon_K$ valence states and $m_K=\dfrac{N_K}{2}$ valence nucleons in the valence space $\Delta\varepsilon_K$, which gives the dimension

$$d(m_1,m_2)=\begin{pmatrix} N_1 \\ m_1 \end{pmatrix}\begin{pmatrix} N_2 \\ m_2 \end{pmatrix}.$$

The local excitation energy is defined as

$$\varepsilon^* = E_{\rm x} - U(A_1, A_2, J). \tag{5}$$

The detailed calculation of the driving potentials can be seen in Ref. [16–18]. The excitation energy $E_{\rm x}$ of the composite system is converted from the relative kinetic energy loss, which is related to the Coulomb barrier B[16] and determined for each initial relative angular momentum J by the parametrization method of the classical deflection function[19−20]. So, $E_{\rm x}$ is coupled with the relative angular momentum.

In Fig. 1(a) we show the interaction potential as a function of the relative distance, for the channel ^{48}Ca+^{244}Pu. Due to the attractive nuclear and repulsive Coulomb forces, there is a pocket and a QF barrier in the potential. QF happens when $r > r_{\rm b}$. Fig. 1(b) shows the PES (the driving potential for nucleon transfer) in the reaction ^{48}Ca+^{244}Pu as a function of the mass asymmetry $\eta = \dfrac{A_1 - A_2}{A_1 + A_2}$, the two nuclei of each DNS are located at the bottom of the pocket. The driving potential has been calculated to cover $\eta = -1$ to 1. The arrow in Fig. 1(b) indicates the entrance channel η_i. One nucleon transfer from η_i to both sides, whether it is a neutron or a proton, depends on in which direction the potential energy is lower. It turns out that the isotopic composition of the nuclei forming the DNS determined in this way does not deviate much from that following the condition of $\dfrac{N}{Z}$ equilibrium in the system. Consequently, the driving potential is an explicit function of neutron and proton numbers of fragments. This is the reason that the driving potential is not symmetric to $\eta = 0$. One may find that in order to form a compound nucleus, a certain amount of energy is needed to pass over the inner fusion barrier at $A_{\rm BG}$, and this is supplied by the incident energy.

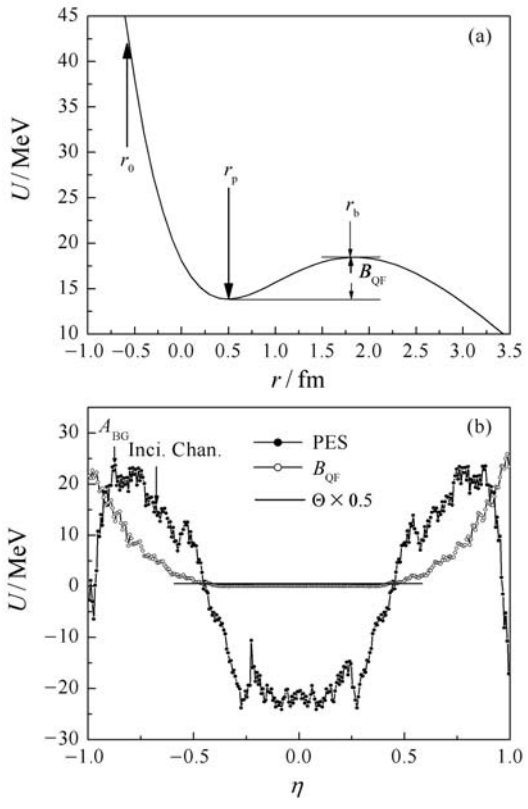

Fig. 1　The interaction potential and PES for the reaction ^{48}Ca+^{244}Pu.

(a) The interaction potential between colliding nuclei as a function of the relative distance variable between the nuclei. (b) The PES(solid line with dotes) as a function of mass asymmetry, the dashed line indicates the QF barrier, and the horizontal line stands for the line with temperature 0.5Θ for a local excitation energy being 30 MeV.

The QF rate $\Lambda^{\rm QF}$ was estimated with the one-dimensional KRA-F[21−22]

$$\Lambda^{\rm QF}(\Theta(t)) = \frac{\omega}{2\pi\omega^{B_{\rm QF}}} \left(\sqrt{\left(\frac{\Gamma}{2\hbar}\right)^2 + (\omega^{B_{\rm QF}})^2} - \frac{\Gamma}{2\hbar} \right) \times \exp\left(-\frac{B_{\rm QF}(A_1, A_2)}{\Theta(t)} \right). \tag{6}$$

Here the QF barrier is counted from the depth of the pocket of the interaction potential(see Fig. 1(a)). The local temperature is given by the Fermi-gas expression $\Theta = \sqrt{\dfrac{\varepsilon^\star}{a}}$ corresponding to the local excitation energy $\varepsilon^\star$ and with the level density parameter $a = \dfrac{A}{12}$ MeV^{-1}. The frequency $\omega^{B_{\rm QF}}$ is the frequency of the inverted harmonic oscillator approximating the interaction potential of two nuclei in R around the top of the QF barrier, and ω is the frequency of the harmonic oscillator approximating the potential in R around the bottom of the pocket. The quantity Γ, which denotes the double average width of the contributing single-particle states, determines the friction coefficients: $\gamma_{ii'} = \dfrac{\Gamma}{\hbar}\mu_{ii'}$, with $\mu_{ii'}$ being the inertia tensor. Here constant values $\Gamma = 2.8$ MeV, $\hbar\omega^{B_{\rm QF}} = 2.0$ MeV and $\hbar\omega = 3.0$ MeV were used. The QF mass yields finally:

$$Y^{\rm QF}(A_1) = \sum_{J=0}^{J_{\max}} \int_0^{\tau_{\rm int}} P(A_1, E_1, t) \Lambda^{\rm QF}(\Theta(t)) {\rm d}t. \tag{7}$$

The interaction time $\tau_{\rm int}$ in the dissipative process of two colliding nuclei is dependent on the incident energy $E_{\rm c.m.}$

and the incident angular momentum J, which is determined by using the deflection function method[20], and has the value of the magnitude from a few to several hundred 10^{-22} s.

4 The diffusion along the distance between nuclei

In order to check the validity of the KRA-F in treating the QF, the relative distance between the centers of nuclei of DNS is taken as an independent dynamical variable in addition to the mass number A_1 of the project-like fragment. In this way, the evolutions of DNS towards the mass asymmetry (the nucleon transfer) to form the compound nucleus, and along the relative distance leads to the QF, both are governed by the same ME.

The ME is set as:

$$\begin{aligned}&\frac{\mathrm{d}P(A_1,R,E^R_{A_1},t)}{\mathrm{d}t}=\\&\sum_{A'_1}W_{A_1,R;\,A'_1,R}(t)[d_{A_1,R}P(A'_1,R,E^R_{A'_1},t)-\\&\qquad d_{A'_1,R}P(A_1,R,E^R_{A_1},t)]+\\&\int_{R_0}^{R_\mathrm{b}}W_{A_1,R;A_1,R'}(t)[d_{A_1,R}P(A_1,R',E^{R'}_{A_1},t)-\\&\qquad d_{A_1,R'}P(A_1,R,E^R_{A_1},t)]\rho(R')\mathrm{d}R'-\\&\int_{R_\mathrm{b}}^{\infty}W_{A_1,R;A_1,R'}(t)d_{A_1,R'}P(A_1,R,E^R_{A_1},t)\rho(R')\mathrm{d}R'\,,\end{aligned}\quad(8)$$

where $P(A_1,R,E^R_{A_1},t)$ denotes the probability distribution function to find fragment 1 with A_1 nucleons, at the relative distance being R with the corresponding local excitation energy $E^R_{A_1}$ at time t, and here R is taken as a discrete variable. It is taken as a continuous variable in the second and third line of Eq. (2). $\rho(R')=\dfrac{1}{h}$ is the density of the discrete dots with the step length h. As mentioned before, the local excitation energy is determined by the dissipated energy from the relative motion and the PES of the corresponding DNS, which is shown in Eqs. (4) and (5). $W_{A_1,R;A'_1,R}(t)=W_{A'_1,R;A_1,R}(t)$ $\big($or $W_{A_1,R;A_1,R'}(t)=W_{A_1,R';A_1,R}(t)\big)$ is the mean transition probability from the channel $(A_1,R,E^R_{A_1})$ to $(A'_1,R,E^R_{A_1})$ $\big($or from $(A_1,R,E^R_{A_1})$ to $(A_1,R',E^{R'}_{A_1})\big)$, and $d_{A_1,R}$ denotes the microscopic dimension corresponding to the macroscopic state $(A_1,R,E^R_{A_1})$. The sum is taken over all possible mass numbers that a fragment A'_1 may take. The integration goes along the distance between the centers of nuclei. To solve the two variable-partial differential equations numerically, a two-step-difference-scheme is adopted, and the simultaneous transition for A_1 and R is not taken. Here we used the notation:

$$r_{0,\mathrm{p},\mathrm{b}}=R_{0,\mathrm{p},\mathrm{b}}-\left[R^0_1\Big(1+\sqrt{\frac{5}{4\pi}}\beta_1\Big)+R^0_2\Big(1+\sqrt{\frac{5}{4\pi}}\beta_2\Big)\right],$$

where R^0_1, R^0_2 are the spherical radii of the two fragments. r_p, r_b stand for the relative distance between nuclei where the interaction potential is at the bottom of the interaction pocket and at the top of the barrier, respectively. r_0 is the distance between nuclei at which the potential is high enough that the probability distribution function to find fragment 1 with A_1 nucleons with the corresponding local excitation energy $E^R_{A_1}$ at time t is essentially zero(See Fig. 1(a)). $R_0, R_\mathrm{p}, R_\mathrm{b}$ correspond to $r_0, r_\mathrm{p}, r_\mathrm{b}$ with above relation. The motion of nucleons in the potential energy surface is governed by a single-particle Hamiltonian[15–18]. The initial condition is: $P(A_\mathrm{P},R_\mathrm{P},E^{R_\mathrm{P}}_{A_\mathrm{P}},t=0)=1$, where A_P is the mass number of the projectile.

The PES of the DNS is given by

$$\begin{aligned}U(A_1,A_2,R,J)=B(A_1)+B(A_2)+V_\mathrm{CN}(A_1,A_2,R,J)-\\\big[B(A_\mathrm{CN})+V^\mathrm{CN}_\mathrm{rot}(J)\big]\,,\end{aligned}\quad(9)$$

where all the notations are the same with those from Eq. (7). The PES of the reaction ^{48}Ca+^{244}Pu is shown in Fig. 2 in two dimensions.

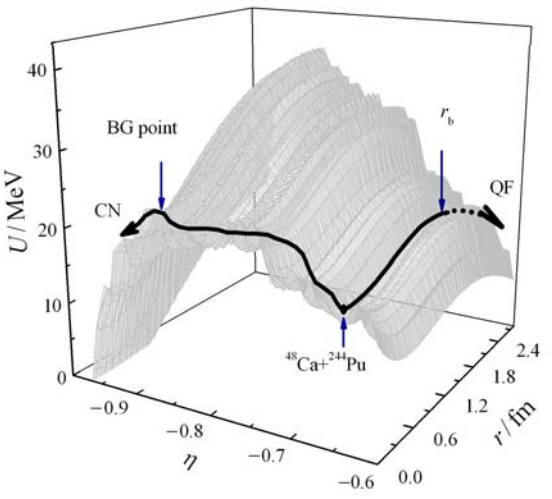

Fig. 2 The PES for the reaction ^{48}Ca+^{244}Pu as a function of mass asymmetry and relative distance variable.

The QF yield is calculated by :

$$Y^\mathrm{QF}_{A_1}(J)=\int_{t=0}^{\tau_\mathrm{int}}\int_{r_\mathrm{b}}^{\infty}P(A_1,r_{A_1},E^r_{A_1}(J),t)\rho(r_{A_1})\mathrm{d}r_{A_1}\mathrm{d}t.\quad(10)$$

The QF mass yields of the reaction ^{48}Ca+^{244}Pu are shown in Fig. 3(a). The dotted line plus circles is calculated by KRA-F, and the solid line with dots is obtained by diffusion calculations(DIFF) with MEs. The QF yields by dissusion calculations are larger than those by KRA-F in the range of $A_1 \leqslant 62$, and smaller in the range of $62 < A_1 \leqslant \left(\frac{A_{\rm CN}}{2} = 146\right)$. Comparing with the results by KRA-F, the results from diffusion calculations show smaller fluctuations in the range of $\left(\frac{A_{\rm CN}}{2} - 80 = 66\right) \leqslant \left(\frac{A_{\rm CN}}{2} - 30 = 116\right)$, and show a little better agreement with the experimental data[21, 23], which are denoted by squares. The KRA-F is a solution of a Fokker-Planck equation under a stationary condition, i.e. under the condition that the probability distribution does not change with time. This condition can not be fulfilled if the barrier is not high enough. In Ref. [10] the application of the Kramers-type expression to relatively small barriers $\frac{B_{\rm QF}}{\Theta} > 0.5$ is mentioned. In Fig. 1(b) the dotted line stands for the QF barrier. It is seen, however, that in the mass symmetric region $-0.48 \leqslant \eta \leqslant 0.48$, which is the region $\left(\frac{A_{\rm CN}}{2} - 70 = 76\right) \leqslant A_1 \leqslant \left(\frac{A_{\rm CN}}{2} + 70 = 216\right)$ for the coordinate A_1, the condition is not fulfilled. While in the mass asymmetric region, where the QF barrier is high, the two calculations with KRA-F and Diffusion are very agreeable. This can be seen in Fig. 3(b). Let us consider the QF barrier with increasing A_1 in Fig. 1(b) from left to right. When the QF barrier is very large, the agreement between the two results is quite good. With decreasing QF barrier, the discrepancies get larger, but the tendencies are still agreeable, which is quite different from their behavior in the mass symmetrical region. This sheds the light on that the KRA-F works well if the barrier is sufficiently high. In the domain of the medium-mass fragments $\left(\frac{A_{\rm CN}}{2} - 30 = 116\right) \leqslant A_1 \leqslant \left(\frac{A_{\rm CN}}{2} + 30 = 176\right)$, the experimental data are higher than the calculated values, because the experimental data contain various contributions: QF fragments, fusion-fission fragments, evaporation residue of heavy excited fragments, fission of heavy fragments, and so on.

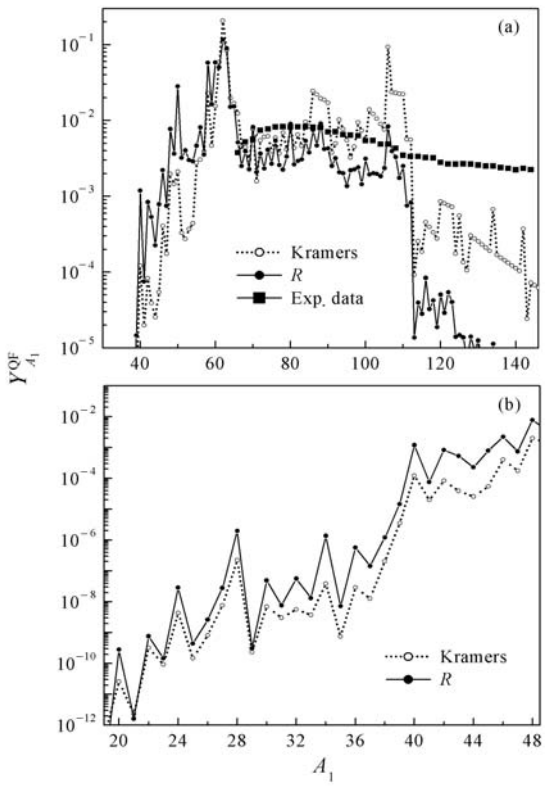

Fig. 3　Mass yields of the reaction ^{48}Ca+^{244}Pu calculated with dissusion and KRA-F, respectively.

The time evolution of the QF mass yields for the reaction ^{48}Ca+^{244}Pu at $E_{\rm c.m.} = 203.32$ MeV (excitation energy of the compound nucleus is 42 MeV) is shown in Fig.4. It is indicated that the QF mass fragments initially are distributed around the entrance channel, then diffuse gradually wider, mainly to the side of heavier mass fragments, since the driven potential favors this way. The equilibrium is reached at about $t = 100 \times 10^{-22}$ s.

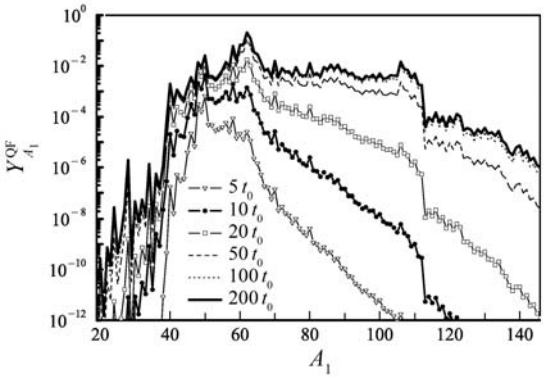

Fig. 4　The time evolution of the mass yields of the reaction ^{48}Ca+^{244}Pu calculated with diffusion with $t_0 = 10^{-22}$ s.

From Figs. 3 and 4 one may find that from $A_1 = 112$ to $A_1 = 113$ the QF mass yield calculated drops down about 3 orders of magnitude. This is due to the structure of the driven potential. The quadrupole deformation parameter of nucleus $A_1 = 112(N_1 = 70)$ is 0.327, and with one proton more for nucleus $A_1 = 113(N_1 = 70)$ the deformation abruptly changes to -0.258. The Coulomb interaction

changes from 266.1 MeV into 278.5 MeV. Thus a peak is formed in the potential at $A_1 = 113$, and accordingly the mass yields decrease. This is shown in Fig. 5(a) and (b) respectively. This reveals the importance of the structure of the driving potential, in which the nuclear deformation, shell and pairing play important roles. By taking the relative distance of nuclei as an independent dynamical variable, the evolution of the DNS towards fusion and QF are both treated as a diffusion process in a consistent way by solving MEs. It is concluded that the KRA-F gives agreeable results with those by the diffusion treatment, if the QF barrier is high enough. Otherwise some large discrepancies occur. Since at the incident fragmentation either for the cold fusion or for the hot fusion, the QF barrier is usually high, and the evolution of the DNS at the incident fragmentation is most important, the KRA-F thus can basically describe the QF in the fusion process.

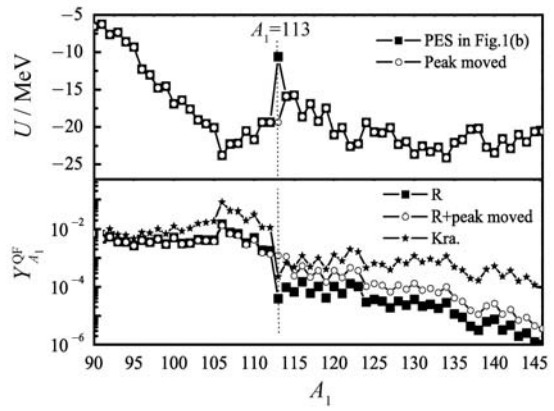

Fig. 5 The driving potential and the QF mass yied of the reaction ^{48}Ca$+^{244}$Pu as a function of the fragment A_1, respectively.
(a) The driving potential of the system, here it is denoted by black squares. The open circles stand for the driving potential, in which the potential value at $A_1 = 113$ is artificially substituted by that of $A_1 = 112$. (b) The mass yields shown by black squares and stars under the driving potential given by black squares in (a) (except at $A_1 = 113$, at all other place the open circles are located on the black squares), calculated by diffusion and KRA-F, respectively. Open circles are the yields distribution under the driving potential by open circles in Fig. 5(a).

5 The effect of the dynamical deformation

In the DNS conception it is assumed that each of the two touching nuclei always keep their own identities with their ground state deformation. However, in the touching configuration, there are nuclear and Coulomb interactions between the nuclei. The nuclei get deformed gradually due to the strong interactions. This dynamical deformation is difficult to describe, and no theory succeeds to describe it so far, since the thorough coupling between the collective and intrinsic variables is impossible for heavy ion reactions. We take the quadrupole deformations of the nuclei in the DNS as dynamical variables in addition to the mass asymmetry variable and construct a new three variable ME so that the deformations as well as the nucleon transfer are viewed as a diffusion process governed by MEs in the PES of the system[24]. The ME is set as:

$$\frac{\mathrm{d}P(A_1,\beta_1,\beta_2,t)}{\mathrm{d}t} = \sum_{A_1'} W_{A_1,\beta_1,\beta_2;A_1',\beta_1,\beta_2}(t)\times$$
$$\Big[d_{A_1,\beta_1,\beta_2}P(A_1',\beta_1,\beta_2,t) - d_{A_1',\beta_1,\beta_2}P(A_1,\beta_1,\beta_2,t)\Big] +$$
$$\int_{\beta_{10}}^{\infty}\int_{\beta_{20}}^{\infty} W_{A_1,\beta_1,\beta_2;\,A_1,\beta_1',\beta_2'}(t)\Big[d_{A_1,\beta_1,\beta_2}P(A_1,\beta_1',\beta_2',t) -$$
$$d_{A_1,\beta_1',\beta_2'}P(A_1,\beta_1,\beta_2,t)\Big]\,\rho(\beta_1')\rho(\beta_2')\mathrm{d}\beta_1'\mathrm{d}\beta_2' -$$
$$\Lambda^{\mathrm{QF}}_{A_1,\beta_1,\beta_2}\big(\Theta(t)\big)P(A_1,\beta_1,\beta_2,t)\,. \qquad (11)$$

One can understand the formula by following the understanding to Eqs. (2) and (12). To solve the three variable-partial differential equations numerically, a three-step-difference-scheme is adopted. The lower limit of deformations is $\beta_{10,20} = 0$ if the initial deformations $\beta_{P,T} > 0$, else $\beta_{10,20} = -0.6$. The tip-to-tip relative orientation is assumed and the nuclei stay in the bottom of the pocket and keep the lowest potential. The KRA-F is used to describe the QF. As mentioned that the KRA-F works well in the mass asymmetry region where the QF barriers are high[25]. The QF yields are finally obtained with

$$Y^{\mathrm{QF}}_{A_1}(J) = \int_{t=0}^{\tau_{\mathrm{int}}}\int_{\beta_{10}}^{\infty}\int_{\beta_{20}}^{\infty}\Lambda^{\mathrm{QF}}_{A_1,\beta_1,\beta_2}\big(\Theta(t)\big)\times$$
$$P(A_1,\beta_1,\beta_2,t)\rho(\beta_1)\rho(\beta_2)\mathrm{d}\beta_1\mathrm{d}\beta_2\mathrm{d}t\,. \qquad (12)$$

The potential energy of the DNS reads:

$$U(A_1,A_2,R,\beta_1,\beta_2,J) =$$
$$E(A_1,\beta_1)+E(A_2,\beta_2)+V_{\mathrm{CN}}(A_1,A_2,R,\beta_1,\beta_2,J) -$$
$$\Big[E(A_{\mathrm{CN}},\beta_{\mathrm{CN}})+V^{\mathrm{CN}}_{\mathrm{rot}}(J)\Big]\,, \qquad (13)$$

where $A_{\mathrm{CN}} = A_1 + A_2$ is the mass number of the compound nucleus, β_i represents the quadrupole deformation of the

two fragments. $E(A_i, \beta_i)$, $(i = 1, 2)$ and $E(A_{\rm CN}, \beta_{\rm CN})$ are the total energies of the ith nucleus and the compound nucleus, respectively, in which the shell and the pairing corrections are included. They can be calculated as a sum of the liquid drop energy and the Strutinsky shell correction. We use the formula and parameters of Ref. [26]:

$$E(A_i, \beta_{i2}) = E_{\rm LD}(A_i)\times \prod_{k=2 \text{ and } 4}\left[(1+b_{ik}\beta_{ik}^2)+c_1 E_{\rm shell}(A_i, \beta_{ik})\right], \qquad (14)$$

where, only axially deformed cases β_{i2} and β_{i4} are considered. The energy of a nucleus with respect to the axial deformations is calculated with a Skyrme energy-density functional together with the extended Thomas-Fermi approximation, which gives the minimum total energies of the ith nucleus with the optimum β_{i2}, β_{i4}. The binding energy and the ground state deformation obtained with this formula are very close to the results in Möller's table[27]. The $V_{\rm rot}^{\rm CN}$ is the rotation energy of the compound nucleus. The interaction potential between the two nuclei $V_{\rm CN}(A_1, A_2, R, \beta_1, \beta_2, J)$ includes the nuclear, Coulomb interaction and centrifugal parts, the details are given in Ref. [16].

The QF mass yields of the reaction ^{48}Ca+^{244}Pu with $E^* = 33$ MeV are showed by solid lines in Fig. 6(c) and (d), obtained by using the one variable ME [11, 18] with the deformation at ground state and by using the current ME with DET, respectively. In Fig. 6(c), there are two high peaks at mass numbers 61 and 106, corresponding to two minima of the PES in Fig. 6(a). This is not consistent with the experimental data. Furthermore, the QF yield falls down about three orders of magnitude at mass number 113 because a high peak appears in the PES in Fig. 6(a) for this mass asymmetry. The reason is that the ground state deformation of the heavy nucleus abruptly changes from 0.328(at $A_1 = 112$) to -0.258(at $A_1 = 113$)[25]. By considering the deformations of the nuclei as dynamical variables, the variation of the deformations is governed by the Eq. (11) in the PES of the system, and the PES is depending on the deformations. Thus we get reasonable deformations. When the deformations reached the equilibrium the PES and QF yields obtained with the current method are shown in Fig. 6(b) and (d), respectively. In the Fig. 6(d) it is seen that the highest peak is at mass number 86 with the heavy fragment close to ^{208}Pb, reflecting the shell effect. It corresponds to a minimum of the PES in Fig. 6(b) and

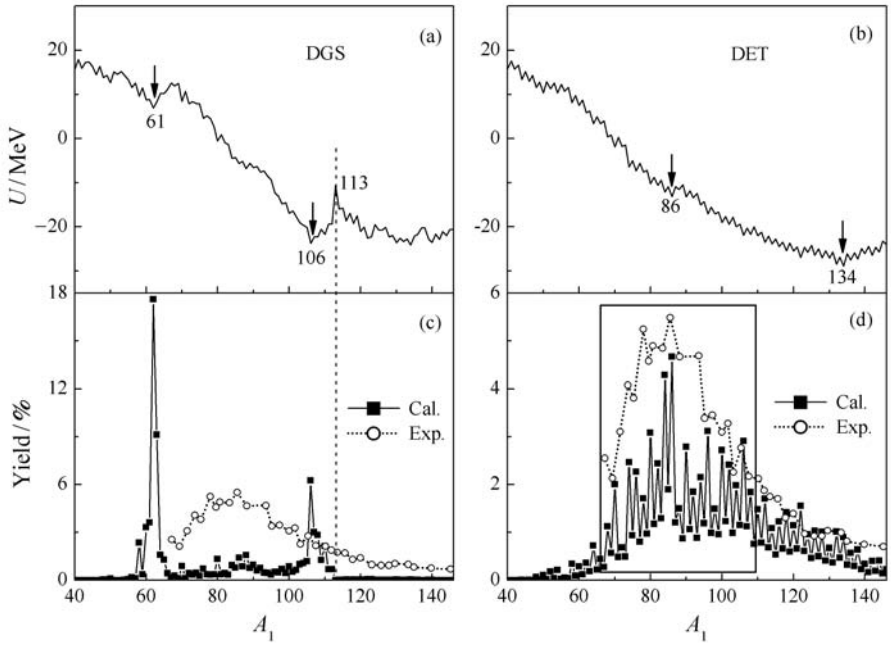

Fig. 6　The PES and QF yields in different conditions for the ^{48}Ca + ^{244}Pu at $E^* = 33$ MeV along the mass asymmetry degree of freedom.
(a) and (c) The PES and QF yields with ground state deformation obtained from the Möller's table, respectively. (b) the PES with the equilibrium deformations (at a large interaction time when the deformations in each mass asymmetry channel have already reached their equilibrium). (d) QF yield with the method of deformations evolving with time(DET). In (c) and (d), the experimental data are denoted by circle.

agrees rather well with the experimental data, although the peak is a little lower than the experimental one. However, in the range of the rectangle, the mass intervals of the experimental points are about 2, and those of our calculated ones are equal 1. On the other hand, the error bars of the data are greater than 2[3, 28]. One should note that the total yields of the data and of our calculation in the rectangle area(mass number from 67 to 104) are 0.612 and 0.656, respectively. The two values are very close.

We also calculated the QF yields of reactions ^{48}Ca$+^{248}$Cm and ^{48}Ca$+^{238}$U with $E^* = 33$ MeV, which are displayed by black squares in Fig. 7(a) and (b), respectively. The highest peaks of the two distributions are at the mass numbers $A_1 = 88$ and $A_1 = 84$, respectively, and fit the data quite well. It is worth to mention that the authors of Ref. [21] found a sharp QF yield peak at $A_1 = 43$ for each of the above mentioned three reactions. This phenomenon does not exist in our results. The dynamical treatment of the system populates the considered dynamical variables correctly. The dynamical deformation of nuclei of the DNS instead of the consideration of the deformation on their ground state can better describe the distribution of the QF yields. This demonstrates the necessity of the consideration of the time-dependent deformation.

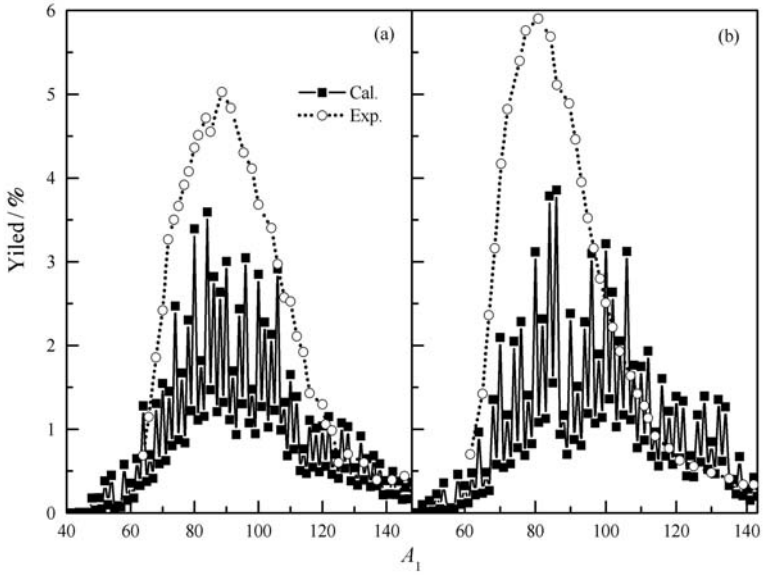

Fig. 7 Mass yields of the reaction ^{48}Ca$+^{248}$Cm (a) and ^{48}Ca$+^{238}$U (b) at $E^* = 33$ MeV compared with the experimental data, respectively.

6 Summary and discussion

The QF in heavy fusing reaction systems is studied within the DNS conception to reveal the reaction mechanism. A two variable ME which include the coupling of the mass asymmetry and the distance between the centers of the nuclei is used to describe the QF mass yield distribution, the shell effect is found, and the agreement with the data is improved. The KRA-F has been used ever since 2001[29], so this is a large step forward, and the validity of the KRA-F is thus checked. It turns out that KRA-F works well if the QF barrier is high enough. Otherwise some large discrepancies occur. In addition to the mass asymmetry variable we treat the quadrupole deformations of the nuclei in the DNS as dynamical variables, and have constructed a new three-variable ME so that the deformations as well as the nucleon transfer are viewed as diffusion processes consistently governed by MEs in the PES. Due to the dynamical treatment the distribution probability of the system is populated reasonably with respect to the considered variables. The calculated QF yield distribution is greatly improved to fit the data.

References:

[1] HOFMANN S. Prog Part Nucl Phys, 2009, **62**(2): 337.

[2] MORITA K, MORIMOTO K, KAJI D, *et al*. J Phys Soc Jpn, 2004, **73**: 2593.

[3] OGANESSIAN Y. J Phys G, 2007, **34**(4): R165.

[4] OGANESSIAN Y, ABDULLIN F S, Bailey P D, *et al*. Phys Rev Lett, 2010, **104**(14): 142502.

[5] ARMBRUSTER P. Annu Rev Nucl Sci, 1985, **35**: 135.

[6] HOFMANN S. Rep Prog Phys, 1998, **61**(6): 639.

[7] HOFMANN S, MÜNZENBERG G. Rev Mod Phys, 2000, **72**(3): 733.

[8] HOFMANN S, HEßBERGER F P, ACKERMANN D, *et al*. Eur Phys J A, 2002, **14**(2): 147.

[9] OGANESSIAN Y T, UTYONKOV V K, LOBANOV Y V, *et al*. Phys Rev Lett, 1999, **83**(16): 3154; OGANESSIAN Y T, YEREMIN A V, POPEKO A G, *et al*. Nature, 1999, **400**: 242; DANILYAN G V, FEDOROV A M, GAGARSKI A M, *et al*. Phys Atom Nucl, 2000, **63**(9): 1671; OGANESSIAN Y T, UTYONKOV V K, LOBANOV Y V, *et al*. Phys Rev C, 2000, **62**(4): 041604(R); OGANESSIAN Y T, UTYONKOV V K, MOODY K J, *et al*. Phys Atom Nucl, **64**(8): 1349.

[10] ADAMIAN G G, ANTONENKO N V, SCHEID W. Nuclear Physics A, 2000, **678**(1/2): 24.

[11] FENG Zhaoqing, JIN Genming, LI Junqing, *et al*. Nuclear Physics A, 2009, **816**(1/4): 33.

[12] FENG Zhaoqing, JIN Genming, LI Junqing, *et al*. Nuclear Physics Review, 2009, **26**(Suppl.1): 168;
FENG Zhaoqing, JIN Genming, LI Junqing. Nuclear Physics Review, 2011, **28**(1): 1.

[13] HUANG Minghui, GAN Zaiguo, FENG Zhaoqing, *et al*. Chin Phys Lett, 2008, **25**(4): 1243.

[14] ADAMIAN G G, ANTONENKO N V, SCHEID W, *et al*. Nucl Phys A, 1998, **633**(3): 409.

[15] FENG Zhaoqing, JIN Genming, FU Feng, *et al*. Nucl Phys A, 2006, **771**: 50.

[16] FENG Zhaoqing, JIN Genming, FU Feng, *et al*. High Ener Phys and Nucl Phys, 2007, **31**(4): 366.(in Chinese)
(冯兆庆，靳根明，付芬，等. 高能物理与核物理，2007，**31**(4): 366.)

[17] LI Wenfei, WANG Nan, LI Junqing, *et al*. Eur Phys Lett, 2003, **64**(6): 750.

[18] LI Wenfei, WANG Nan, JIA Fen, *et al*. J Phys G, 2006, **32**(8): 1143.

[19] WOLSCHIN G, NÖRENBERG W. Z Phys A, 1978, **284**(2): 209.

[20] LI Junqing, WOLSCHIN G. Phys Rev C, 1983, **27**(2): 590.

[21] ADAMIAN G G, ANTONENKO N V, SCHEID W. Phys Rev C, 2003, **68**(3): 034601.

[22] GRANG Pé, LI Junqing, WEIDENMÜLLER H A. Phys Rev C, 1983, **27**(5): 2063.

[23] ITKIS M G, BOGACHEV A A, ITKIS I M, *et al*. Nucl Phys A, 2004, **734**: E13.

[24] HUANG Minghui, ZHANG Zhiyuan, GAN Zaiguo, *et al*. Phys Rev C, 2011, **84**(6): 064619.

[25] HUANG Minghui, GAN Zaiguo, ZHOU Xiaohong, *et al*. Phys Rev C, 2010, **82**(4): 044614.

[26] WANG Ning, LIU Min, WU Xizhen. Phys Rev C, 2010, **81**(4): 044322.

[27] MÖLLER P, NIX J, MYERS W, *et al*. At Data and Nucl Data Tables, 1995, **59**: 185.

[28] ITKIS M G, BOGACHEV A A, ITKIS I M, *et al*. Nucl Phys A, 2007, **787**(1/4): 150.

[29] DIAZ-TORRES A, ADAMIAN G G, ANTONENKO N V, *et al*. Phys Rev C, 2001, **64**(2): 024604.

重离子熔合反应系统中的准裂变

郁 琳[1, 2]，甘再国[1]，黄明辉[1]，张鸿飞[3]，李君清[1, 3]

(1. 中国科学院近代物理研究所，甘肃 兰州 730000;
2. 中国科学院大学，北京 100049;
3. 兰州大学核科学与技术学院，甘肃 兰州 730000)

摘要： 在重离子熔合反应中，准裂变与熔合过程之间相互竞争。在双核模型中，常常在主方程中加入Kramers公式来描述准裂变。但只有当准裂变位垒足够高时，该公式才能成立。在本工作中，把弹靶核的间距作为独立的动力学变量，通过求解主方程来自洽地同时描述双核模型向全熔合和准裂变过程的演化，因此检验了Kramers公式的适用条件。此外，在重离子熔合反应过程中，把动力学形变的演化和核子的转移过程都看成是耗散过程，在系统的势能面的约束下，同时求解含有动力学形变参量和质量不对称度参量的一系列主方程。研究显示了动力学形变对准裂变质量分布的直接影响，得到了与实验观测值符合得很好的计算结果。

关键词： 超重核；准裂变；熔合；主方程；驱动势

收稿日期：2012-12-10；　**修改日期：**2013-06-14

基金项目：国家自然科学基金资助项目(11120101005，11175074，11105035，10805061，10825522,10975064)；中国科学院知识创新工程重大项目(KJCX2-EW-N01)，国家重点基础研究发展计划项目(973计划)(2007CB815000)

通信作者：李君清，E-mail: jqli@impcas.ac.cn